



THE UNIVERSITY *of* EDINBURGH

Edinburgh Research Explorer

Design of the multi-cylinder Stirling engine arrangement with self-start capability and reduced vibrations

Citation for published version:

Daoud, J & Friedrich, D 2019, 'Design of the multi-cylinder Stirling engine arrangement with self-start capability and reduced vibrations', *Applied Thermal Engineering*.

Link:

[Link to publication record in Edinburgh Research Explorer](#)

Document Version:

Peer reviewed version

Published In:

Applied Thermal Engineering

General rights

Copyright for the publications made accessible via the Edinburgh Research Explorer is retained by the author(s) and / or other copyright owners and it is a condition of accessing these publications that users recognise and abide by the legal requirements associated with these rights.

Take down policy

The University of Edinburgh has made every reasonable effort to ensure that Edinburgh Research Explorer content complies with UK legislation. If you believe that the public display of this file breaches copyright please contact openaccess@ed.ac.uk providing details, and we will remove access to the work immediately and investigate your claim.



1 Design of the multi-cylinder Stirling engine arrangement with self-start 2 capability and reduced vibrations

3 Jafar M. Daoud, Daniel Friedrich*

4 *School of Engineering, Institute for Energy Systems, University of Edinburgh, EH9 3DW (Scotland)*

5 *Corresponding author Email: d.friedrich@ed.ac.uk

6 **Abstract:** *The Franchot engine is a double acting Stirling engine that has a freely controllable phase angle and*
7 *no shuttle and axial conduction losses but is inferior to the Siemens and free piston Stirling engines in terms of*
8 *its ability to self-start. In addition, the Franchot engine is not widely used with the reliable slider crank mechanism*
9 *due to vibrations. Here, the multi-cylinder Franchot engine is thermodynamically and mechanically studied with*
10 *the simple slider crank mechanism with the aim of improving the self-start capability and to reduce the vibrations.*
11 *Both instantaneous power and engine arrangements are used to judge the mechanical performance for different*
12 *engine parameters and configurations. The optimal phase shifts and phase angles are derived and it is shown*
13 *that both are governed by the number of cylinders. The theoretical analysis shows that by increasing the number*
14 *of cylinders, different engine vibrations are reduced and the engine becomes self-starting. Hence, the Franchot*
15 *engine can be superior to the Siemens engine, particularly due to the ability to remove the rocking couples for*
16 *engines with more than two phases. Thus, the engine operation is stabilised and the simple slider crank*
17 *mechanism can be used with the multi-cylinder Franchot engine.*

18 **Keywords:** *Franchot engine; Stirling engine, double acting; multi-cylinder; phase angle; mechanical vibrations;*

19 1 Introduction

20 The Franchot engine which is a double acting Stirling engine was invented in the 19th century by
21 Charles Louis Franchot [1]. In contrast to the double acting Siemens configuration, only two pistons
22 are required, the phase angle can be freely controlled and each cylinder is either hot or cold which
23 eliminates the shuttle and axial conduction losses [2]. It has been reported that, to complete the
24 thermodynamic cycle in the Siemens configuration, at least three cylinders are needed to achieve the
25 same phase angle between all hot and cold spaces [3][4][5]. This Siemens configuration produces
26 consistent and continuous power through a cycle and hence can be self-starting. This self-starting
27 capability is a significant advantage over the Franchot engine [6].

28 The number of cylinders affects the phase angle and phase shift of the Siemens engine. The phase
29 angle is the thermodynamic angle between each expansion space and its corresponding compression
30 space while the phase shift represents the angular distance between the expansion spaces. For each
31 cylinder thermodynamically connected to an adjacent cylinder, the phase angle is given by

32 $\theta = 180^\circ - \frac{360^\circ}{N}$ and the phase shift between reciprocating pistons is given by
33 $\theta_s = \frac{360^\circ}{N}$. Here, N is the number of cylinders.

34 Chatterton and Pennacchi [7] showed that different thermodynamic connections can be made
35 between multiple single acting engines with more than four cylinders which result in different phase
36 angles. In addition, the net power increases with the number of engines, while the torque and
37 rotational speed oscillations decrease. Similarly, multi-cylinder double acting engines can have more
38 than one phase angle if each cylinder can be connected to any other cylinder and not only to adjacent
39 cylinders. However, for any Stirling machine the preferred phase angle is within the range 90°-140°
40 [8]. In this range of angles, the Siemens engine with a minimum of four cylinder is needed. At the
41 phase shift of 120°, which can be obtained with the 3-cylinder engine, a non-recommended phase
42 angle equal to 60° is obtained.

43 The thermodynamic cycle is complete for the Franchot engine with only one hot and one cold cylinder
44 with an arbitrary phase angle, which is unconstrained by the configuration. It has not been reported
45 that the single Franchot engine can be self-starting. However, it has been shown [9][10][11] that a
46 dual Franchot engine could self-start if the two engines are phase shifted by 90° , which is equivalent
47 to the four cylinder Siemens configuration in terms of number of cylinders and phase shift. Arthur and
48 Varela [9] patented a dual Franchot engine for a hybrid automotive. They suggested using dual
49 Franchot engines working at the highest efficiency to drive a linear alternator to generate electricity.
50 They suggested a synchronising crank to keep the volume and phase angles at the predefined value of
51 90° . The SPP 4-106 engine [10] is a dual Franchot engine which uses the slider crank drive with a 90°
52 phase shift between the two Franchot engines but can use different phase angles. The 90° phase shift
53 gives the lowest torsional vibration and causes the engine to self-start. Fette [11] manufactured a
54 liquid piston type dual Franchot engine. In which, all liquid pistons were phase shifted by 90° using
55 external solid pistons with a kinematic drive.

56 Double acting as well as single acting Stirling engines can use the simple slider crank drive [12][3] but
57 at the cost of vibrations. The Franchot and dual Franchot engines have an uneven distribution of
58 masses and cranks, which creates dynamic imbalances. These imbalances cause first order vibrations
59 such as reciprocal vibration (i.e. those caused by the up and down piston motion) and rocking couples
60 (i.e. those created due to the offset between pistons). Rocking couples are opposite force twins that
61 cause force moment responsible for the vibration along the crankshaft. Reciprocal vibrations and
62 rocking couples are found in single acting Stirling engines due to the phase angle while rocking couples
63 are found in the Siemens configuration as a result of the absence of piston pairs. Thus, the Siemens
64 engine was brought to practice with the swash plate and wobble yoke [6][13][14]. The wobble yoke
65 has been commercialised at the maximum possible number of cylinders of 4 [7]. Walker [1] suggested
66 using the wobble drive with the Franchot engine for railway applications. Due to the uneven
67 distribution of pistons the Stiller drive is reported to be used with the dual Franchot engine with a
68 phase shift of 90° [15]. In addition, the Stirling engines vibrations can be reduced by methods of
69 reducing the charge pressure or dynamic balancing which adds counterweights to the crankshaft
70 [16][17]. Dynamic balancing can effectively remove vertical vibrations but creates horizontal
71 vibrations hence there will be a need to reduce the reciprocating masses [18][19].

72 Alternatively, in internal combustion engines, vibrations due to the primary forces, which have the
73 same frequency as the engine rotation can be removed by an inherent balance, in which many
74 cylinders participate in generating opposite vibrations that cancel each other out [20]. For example,
75 the reciprocal vibration caused by a moving piston can be eliminated by another piston moving exactly
76 opposite to the first piston. For a three-piston engine, reciprocal vibrations are reduced if the pistons
77 are apart by 120° degree. However, rocking couples still exist due to the offset between pistons. For
78 the 4-cylinder engine, two pistons in the middle move with each other while the outer pistons move
79 with each other and opposite to the middle couple. Hence, reciprocal and rocking vibrations are
80 reduced. Moreover, torsional vibration caused by power pulses on the crankshaft are reduced due to
81 uniform distribution of power strokes. To the best of the authors' knowledge, inherent balance has
82 not been applied to Stirling engines yet. The rocking couples can be removed by piston pairs moving
83 together. While this could be achieved for the Franchot engine, it is not possible for the Siemens
84 engine. Attribution is made to the Siemens engine because it is a multi-cylinder and double acting
85 engine which is preferable over the Franchot engine for its ease of sealing, simpler kinematics and
86 self-starting capability.

87 In their attempt to get rid of complex heat exchangers, Daoud and Friedrich [21] suggested a new heat
88 exchanging mechanism for which, heat is added and rejected directly through the cylinder walls of the

89 Franchot engine. Their polytropic model considers heat addition and removal during the expansion
 90 and compression processes hence they are not isothermal or adiabatic but polytropic. Later, the same
 91 authors [22] proposed hot and cold isothermalisers for the Franchot engine to increase the power and
 92 efficiency and reduce the gas flow rate which helps in reducing the pumping losses. They modified the
 93 polytropic model to include the gas friction losses and enhanced heat transfer in the cylinders and
 94 found that the gas friction can be ignored up to the maximum power. However, increasing the number
 95 of cylinders can lead to an increase in the power similar to the isothermalisers which have some
 96 geometric limitations. Recently, Daoud and Friedrich [23] proposed a new free piston Franchot engine
 97 based on the balanced compounding technique using multiple cylinders. They used a dynamic model
 98 based on the polytropic model and showed that, the free piston Franchot engine is possible and can
 99 use long cylinders with small bores. However, there is a lack of experimental and theoretical research
 100 on the self-starting and vibration reduction of Stirling engines and especially kinematic Stirling engines
 101 [23][24].

102 In this theoretical study, we derive guidelines for the design multi-cylinder Franchot engines with
 103 improved mechanical performance of the kinematic engine. The study uses a validated polytropic
 104 model and phasor diagrams to evaluate the power pulses and mechanical piston arrangements of
 105 multi-cylinder Franchot engines. The results enable the design of multi-cylinder engines with the
 106 simple slider crank drive, which have the capability to self-start and have reduced torsional and
 107 primary vibrations on the crankshaft.

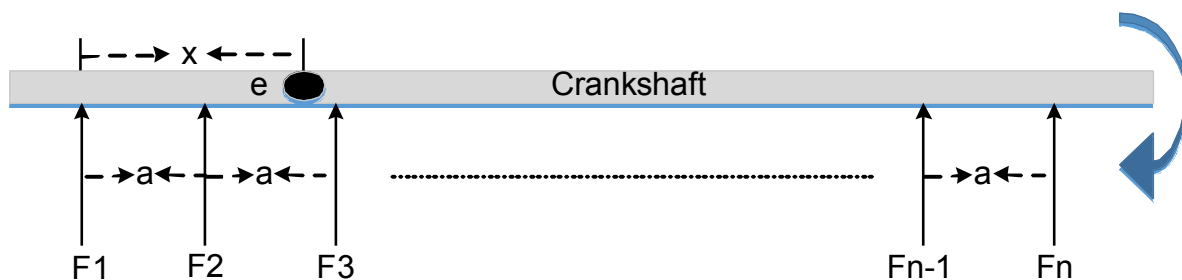
108 2 Methodology

109 A kinematic Stirling engine can start up if the total work over a complete cycle is positive [24]. A single-
 110 acting Stirling engine with kinematic drive generates negative power durations due to the
 111 compression stroke. To guarantee the power hence motion continuity, a flywheel is commonly used
 112 to overcome the negative power durations and reduce generated harmonics by using some of its
 113 stored kinetic energy [25]. At engine start-up, an external mechanical force is required to bring the
 114 engine above the stalling speed. If the force is not adequate the engine will slow down until it
 115 completely stops. The stored energy in a solid cylinder flywheel is given by:

$$k_e = 0.5 J \omega^2 \quad 1$$

116

117 where J and ω are the flywheel moment of inertia and angular velocity, respectively.



118

119 *Figure 1: Free body diagram of a rotating crankshaft showing piston forces.*

120 Here, a strict assumption is made that not only the average power should be positive but also the
 121 instantaneous power generated by the engine should always be positive. This implies that the average
 122 power is positive and the engine starts up at low speeds at which the kinematic energy of the flywheel
 123 is negligible, thus leads to self-starting. The instantaneous power will be used to check the power

124 continuity and power pulses that cause torsional vibrations on the crankshaft of a slider crank
 125 mechanism without using a flywheel. The reciprocal and rocking vibrations will be investigated
 126 according to the inherent balancing method based on the phasor diagram and cylinder arrangement.
 127 A rotating shaft is dynamically balanced if it is statically balanced and the resulting turning moment is
 128 zero which is obtained if there is a uniform distribution of moving masses on the crankshaft. To remove
 129 the rocking couples in the inline topology, the algebraic sum of the couples at any point in the plane
 130 of cylinders should be zero. If the offset between force signals along the crankshaft is the same (see
 131 Figure 1), the force moment at any point on the crankshaft is written as

$$\sum M_e = 0 \quad 2$$

132 hence,

$$\vec{F}_1 x + \vec{F}_2(x - a) + \vec{F}_3(x - 2a) \dots + \vec{F}_n(x - (n - 1)a) = 0 \quad 3$$

133 When the pistons are pairwise coupled (i.e. $\vec{F}_1 = \vec{F}_n, \vec{F}_2 = \vec{F}_{n-1}, \dots$), Equation 3 becomes

$$\vec{F}_1(2x - (n - 1)a) + \vec{F}_2(2x - (n - 1)a) + \dots = 0 \quad 4$$

134 hence,

$$(2x - (n - 1)a) \sum_{i=1}^{n/2} \vec{F}_i = 0 \quad 5$$

135 Thus, to eliminate the vibrations due to rocking couples, piston couples should exist, the offset
 136 between pistons needs to be the same and the vector summation of the primary forces must be zero
 137 which implies that the moving masses have to be uniformly distributed around the crank shaft.

138 The ideal instantaneous power is given by

$$P_{ins} = (p - p')(\dot{v}_e + \dot{v}_c) \quad 6$$

139

140 where p, P, v_e and v_c represent the instantaneous pressure, instantaneous power, expansion volume
 141 and compression volume and the notation ($'$) represents the variables of the opposite piston side.

142 The compression volume of the Franchot engine is calculated from

$$v_c = 0.5 V_{sw}(1 + \cos(\omega t + \theta_s)) + V_{dead} \quad 7$$

143

144 correspondingly, the expansion volume is calculated from

$$v_e = 0.5 V_{sw}(1 + \cos(\omega t + \theta + \theta_s)) + V_{dead} \quad 8$$

145

146 where θ, θ_s, V_{sw} and V_{dead} are the phase angle, phase shift between a Franchot engine and an
 147 arbitrary zero position, swept volume and dead volume, respectively. The swept and dead volume are
 148 calculated from

$$V_{sw} = \frac{\pi D^2}{4} L \quad 9$$

$$V_{dead} = \frac{\pi D^2}{4} r \quad 10$$

149 where, D, L and r are the piston diameter, stroke length and clearance volume, respectively. As the
 150 swept volumes are sinusoidal, Equation 6 can be written as

$$= p(\dot{v}_e + \dot{v}_c) + p'(\dot{v}_e + \dot{v}_c) = P + P' \quad 11$$

151

152 The total power transferred to the crankshaft of a Franchot engine (see Figure 5) is the summation of
 153 power generated by Stirling engines on both sides of the power piston. Assuming the engine is
 154 symmetrical for both sides, the power of the opposite Stirling engine is the power of a Stirling engine
 155 shifted by 180° . Hence, the instantaneous power of the Franchot engine can be calculated by
 156 considering only one side of the Franchot engine as

$$P_{ins} = p(\dot{v}_e + \dot{v}_c) + p(\dot{v}_e + \dot{v}_c)\angle 180^\circ \quad 12$$

157

158 where the second part of the equation is the instantaneous power of a Stirling engine shifted by 180°
 159 (indicated by $\angle 180^\circ$ according to notation for multiphase systems).

160 Similarly, the instantaneous power of any Franchot engine in a multi-engine configuration can be
 161 obtained based on the phasor diagram for different phase shifts without rebuilding distinct equations
 162 for each engine by

$$P_{ins} = [p(\dot{v}_e + \dot{v}_c) + p(\dot{v}_e + \dot{v}_c)\angle 180^\circ]\angle \theta_s \quad 13$$

163 for

$$0^\circ \leq \theta_s \leq 360^\circ \quad 14$$

164

165 By considering only one alpha engine, the number of variables, complexity of the model and the
 166 simulation time are reduced. The pressure variation on one side of the direct cylinder heated and
 167 cooled Franchot engine is calculated from [21]

$$\dot{p} = \frac{-p\left(\frac{\dot{v}_e}{T_{re}} + \frac{\dot{v}_c}{T_{cr}}\right) + \frac{R}{c_p}\left(\frac{\dot{Q}_e}{T_{re}} + \frac{\dot{Q}_c}{T_{cr}}\right)}{\frac{v_e}{\gamma T_{re}} + \frac{V_r}{T_r} + \frac{v_c}{\gamma T_{cr}}} \quad 15$$

168

169 where $v, T, and \dot{Q}$ denote the volume, temperature and heat flow rate in the working spaces,
 170 respectively, and subscripts e, r and c indicate the expansion, regeneration and compression space,
 171 respectively.

172 Regenerator end temperatures are calculated from [21]

$$T_{rh} = \frac{-\phi i \dot{m}_e T_e}{\phi(1-i)\dot{m}_e} \quad 16$$

173

$$T_{rk} = \frac{-\phi j \dot{m}_c T_c}{\phi(1-j)\dot{m}_c} \quad 17$$

174

175 where the parameters i and j are given by

$$i = \begin{cases} 1, & \dot{m}_e < 0 \\ 0, & \dot{m}_e \geq 0 \end{cases} \quad 18$$

176

$$j = \begin{cases} 1, & \dot{m}_c < 0 \\ 0, & \dot{m}_c \geq 0 \end{cases} \quad 19$$

177

178 Hence, the average regenerator temperature is

$$T_r = \frac{T_{rh} - T_{rk}}{\ln \frac{T_{rh}}{T_{rk}}} \quad 20$$

179

180 External irreversibility is considered through the heat addition and removal which are calculated from
181 Newton's law of cooling [26]

$$\dot{Q} = hA\Delta T \quad 21$$

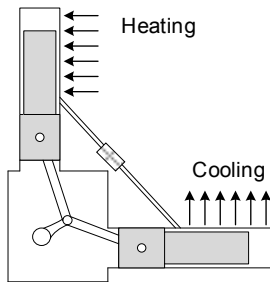
182

183 where h is the convective heat transfer coefficient, which holds for Reynolds' numbers between 1000
184 and 100,000 and is calculated as [27]

$$\begin{aligned} h_e &= 0.042D_h^{-0.42}v^{0.58}p^{0.58}T^{-0.19} \\ h_c &= 0.0236D_h^{-0.47}v^{0.53}p^{0.53}T^{-0.11} \end{aligned} \quad 22$$

185

186 where ΔT , D_h , h_e and h_c are the temperature difference between the working gas and cylinder wall,
187 hydraulic diameter, convective heat transfer during the expansion and compression, respectively.



188

189 *Figure 2: Schematic of the Karabulut alpha type engine with annular heat exchangers.*

190 For validation, the polytropic model is applied to the alpha type engine with annular heat exchanger
191 made by Karabulut [28]. In the Karabulut engine shown in Figure 2, the heat exchanging area and
192 volume are constant for the annulus and dynamic for the swept space. These conditions are replicated
193 in the model for validation purpose. The technical specification of the engine is shown in *Table 1*.

194

Table 1: Technical specifications and operating conditions of Karabulut engine [28].

<i>Name</i>	<i>Value and unit</i>
<i>Stroke length</i>	<i>6 cm</i>
<i>Bore diameter</i>	<i>5.24 cm</i>
<i>Piston dome diameter</i>	<i>4.74 cm</i>
<i>Hot annulus length</i>	<i>13.5 cm</i>
<i>Cold annulus length</i>	<i>11 cm</i>
<i>Connecting pipe length</i>	<i>30 cm</i>
<i>Connecting pipe diameter</i>	<i>0.5 cm</i>
<i>Regenerator matrix</i>	<i>Woven wire</i>
<i>Wire diameter</i>	<i>100 micron</i>

<i>Regenerator porosity</i>	<i>0.7</i>
<i>Regenerator volume</i>	<i>12 cm³</i>
<i>Out-of-Phase angle</i>	<i>90°</i>
<i>Hot, cold temperatures</i>	<i>1100°C, 20°C</i>
<i>Working gas</i>	<i>Air</i>
<i>Average gas pressure</i>	<i>1 bar, 2 bar</i>

195 To increase the accuracy of the model the reheat and pressure losses of the regenerator are
196 considered. The effect of having imperfect regeneration is considered by modifying the regenerator
197 gas stream temperatures as [29][30]

$$T_{rho} = T_{rk} + \varepsilon(T_{rh} - T_{rk}) \quad 23$$

$$T_{rko} = T_{rh} - \varepsilon(T_{rh} - T_{rk}) \quad 24$$

198 where, T_{rho} , T_{rko} and ε are the hot outlet gas temperature, cold outlet gas temperature and
199 regenerator effectiveness, respectively.

200 The effectiveness is calculated according to Tanaka [31] by

$$\varepsilon = \frac{Ntu}{Ntu + 2} \quad 25$$

201 where Ntu is the number of transfer units and calculated from

$$Ntu = \frac{4\overline{Nu}L_r}{P_r\overline{Re}d_h} \quad 26$$

202 where \overline{Nu} , P_r , \overline{Re} and d_h are the average Nusselt number, Prandtl number, average Reynolds number
203 and regenerator hydraulic diameter, respectively.

204 The Nusselt number is correlated according to Tanaka as follows

$$\overline{Nu} = 0.33\overline{Re}^{0.67} \quad 27$$

205 The pressure loss due to the gas friction with the regenerator material is calculated from

$$\Delta p_{loss} = -\frac{0.5f_h\rho L_r U_{max}^2}{d_h} \quad 28$$

206 where Δp_{loss} is the pressure loss and f_h is the friction factor calculated according to Tanaka from

$$f_h = 1.6 + \frac{175}{Re_{max}} \quad 29$$

207 The pressure loss due to the connecting pipe is calculated as

$$\Delta p_{loss} = -\frac{2f_{Re}\mu L_r U_{av}}{d_h} \quad 30$$

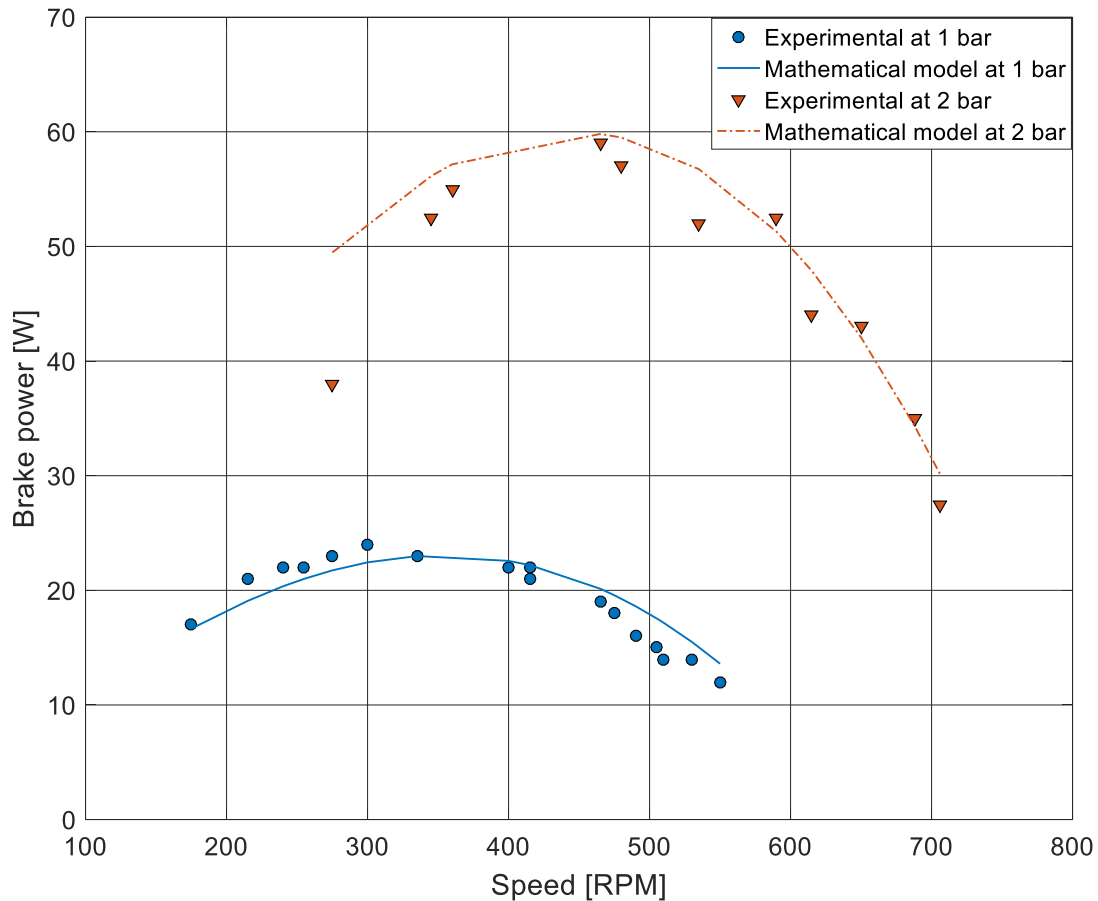
208 where f_{Re} is calculated by [32]

$$f_{Re} = \begin{cases} 16 & Re < 2000 \\ 7.343 * 10^{-4} Re^{1.3142} & 2000 < Re < 4000 \\ 0.0791 Re^{0.75} & Re > 4000 \end{cases} \quad 31$$

209 The model is implemented in Matlab/Simulink and the ordinary differential equations 15 and 21 are
210 solved with the Runge-Kutta method with a time step of 10^{-4} s. A number of simulations at different
211 frequencies was performed with a time step of 10^{-5} s. These showed only negligible differences so that
212 the time step of 10^{-4} s was used for all simulations.

213 The mathematical model is applied to the Karabulut engine at a range of speeds and two pressures.
214 The comparison between the polytropic model and experimental study is shown in Figure 3. The
215 polytropic model has reasonably good agreement with the experimental results especially in

216 predicting the trend of engine performance and location of the power peak values. The maximum
 217 relative error was calculated as 22% and 30% for the 1 and 2 bar data sets, respectively. Those errors
 218 can be attributed to the roughness of the experimental data, the lack of data about gas leakage and
 219 mechanical friction. In addition, these errors are located far away from the power peak operation.
 220 Thus, this validation gives confidence that the polytropic model can accurately predict the operating
 221 conditions and power peak of the Franchot engine.



222
 223 *Figure 3: Comparison between the 3 control volume polytropic model with regenerator losses and experimental data of*
 224 *Karabulut alpha type engine [28].*

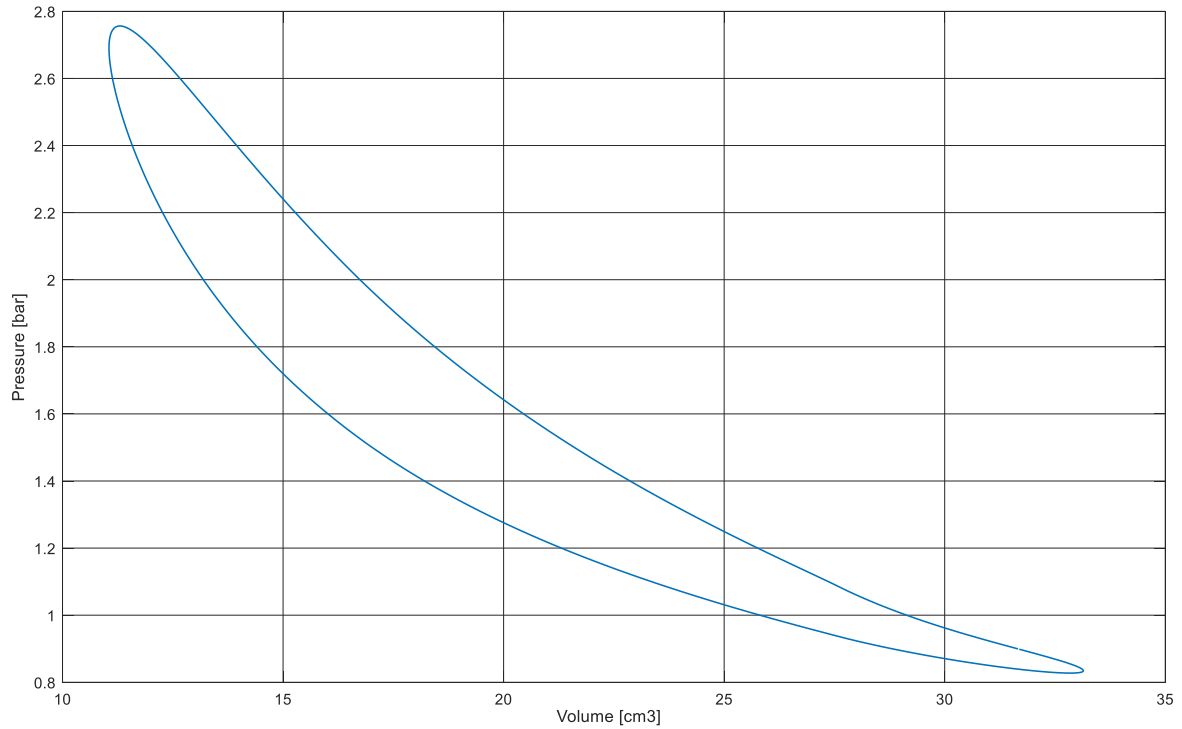
225 3 Results and discussion

226 The reported instantaneous powers were generated once the simulation reached the quasi-steady
 227 state condition. All results use the reference engine parameters listed in Table 2 unless otherwise
 228 stated. The PV diagram of the studied engine is shown in Figure 4.

229 *Table 2: Parameters of the reference engine*

Name	symbol	value/unit
Stroke length	L_e, L_c	50 cm
Bore diameter	D_e, D_c	0.75 cm
Gas density	ρ	1.225 kg/m ³
Clearance length	r_e, r_c	0.1 mm
Reg. volume	V_r	0 cm ³
Phase angle	θ	120°
Temperatures	T_h, T_k	450 K, 300 K

Rotation speed	n	500 RPM,
Working gas	Air	
Gas constant	R	287 J/kg.K



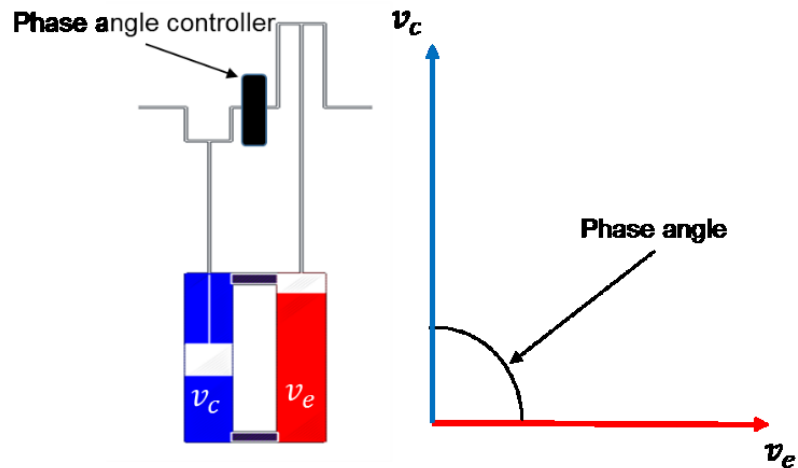
230

231

Figure 4: PV diagram of the reference engine.

232 **3.1 Single phase (1-ph) Franchot engine**

233 This is the simplest engine configuration that has only a pair of hot and cold cylinders connected to
 234 each other by two regenerators. The expansion volume v_e is always leading the compression volume
 235 v_c by an arbitrary phase angle. The phasor diagram of the 1-ph Franchot engine in Figure 5 shows that
 236 forces and masses are not uniformly distributed around the crankshaft, which causes vibrations. The
 237 phase angle controller is used to define the optimal phase angle between the expansion and
 238 compression spaces which is one of the advantages of the Franchot engine over the Siemens engine.
 239 While the masses will be uniformly distributed at a phase angle of 180°, the total engine volume
 240 (expansion, compression and dead volume) for each Stirling engine is constant and the engine will
 241 stall.

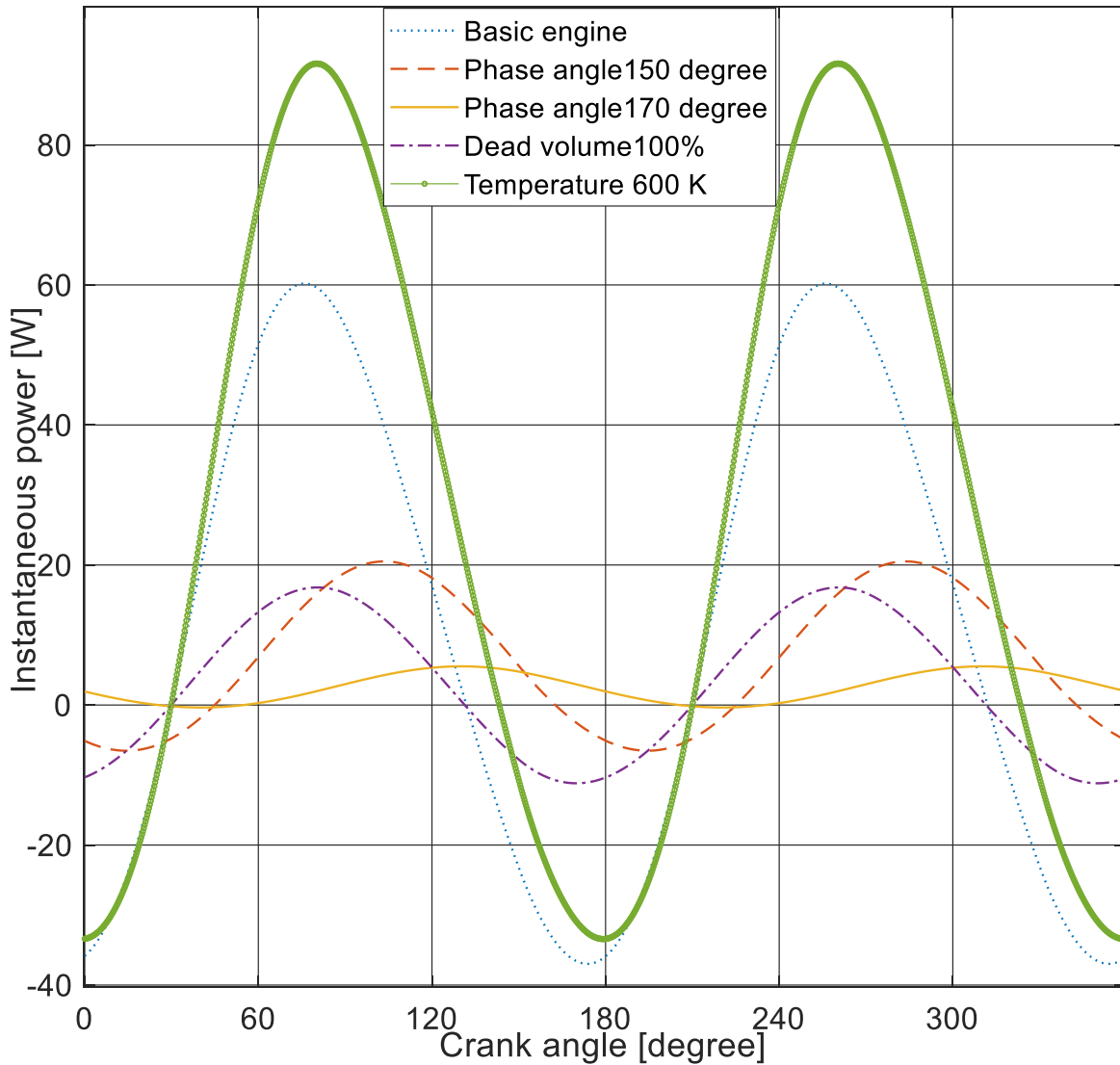


242

243

Figure 5: 1-ph kinematic Franchot engine and its phasor diagram.

244 The start-up capability of the Franchot engine is investigated with respect to the temperature, phase
 245 angle and dead volume (the clearance volume in the engine cylinders). Figure 6 shows that negative
 246 power is reduced but not eliminated for the studied cases. Increasing the temperature increases the
 247 power variation and reduces the negative part of the power by shifting the power curve up due to the
 248 increasing pressure in the expansion stroke. Increasing the dead volume to 100% of the swept volume
 249 reduces the power variations which is due to the reducing pressure variations. Increasing the phase
 250 angle leads to a reduction in the negative part of the power signal without eliminating it completely.
 251 The reduction is due to the decreasing pressure variation and time shift between negative and positive
 252 power peaks. The latter works as a filter for the power signal while reducing the pressure variation
 253 reduces the power signal amplitude so that it oscillates around zero as the volumes on both sides of
 254 the working pistons approach equality. Thus, an increase in the dead volume increases the impact of
 255 the negative power durations. It can be concluded that the 1 – ph Franchot engine does not have the
 256 capability to self-start or run without a flywheel by increasing the input temperature, dead volume or
 257 phase angle.



258

259

Figure 6: Power Response for increasing the phase angle, dead volume and temperature of the reference engine.

260

261

262

263

264

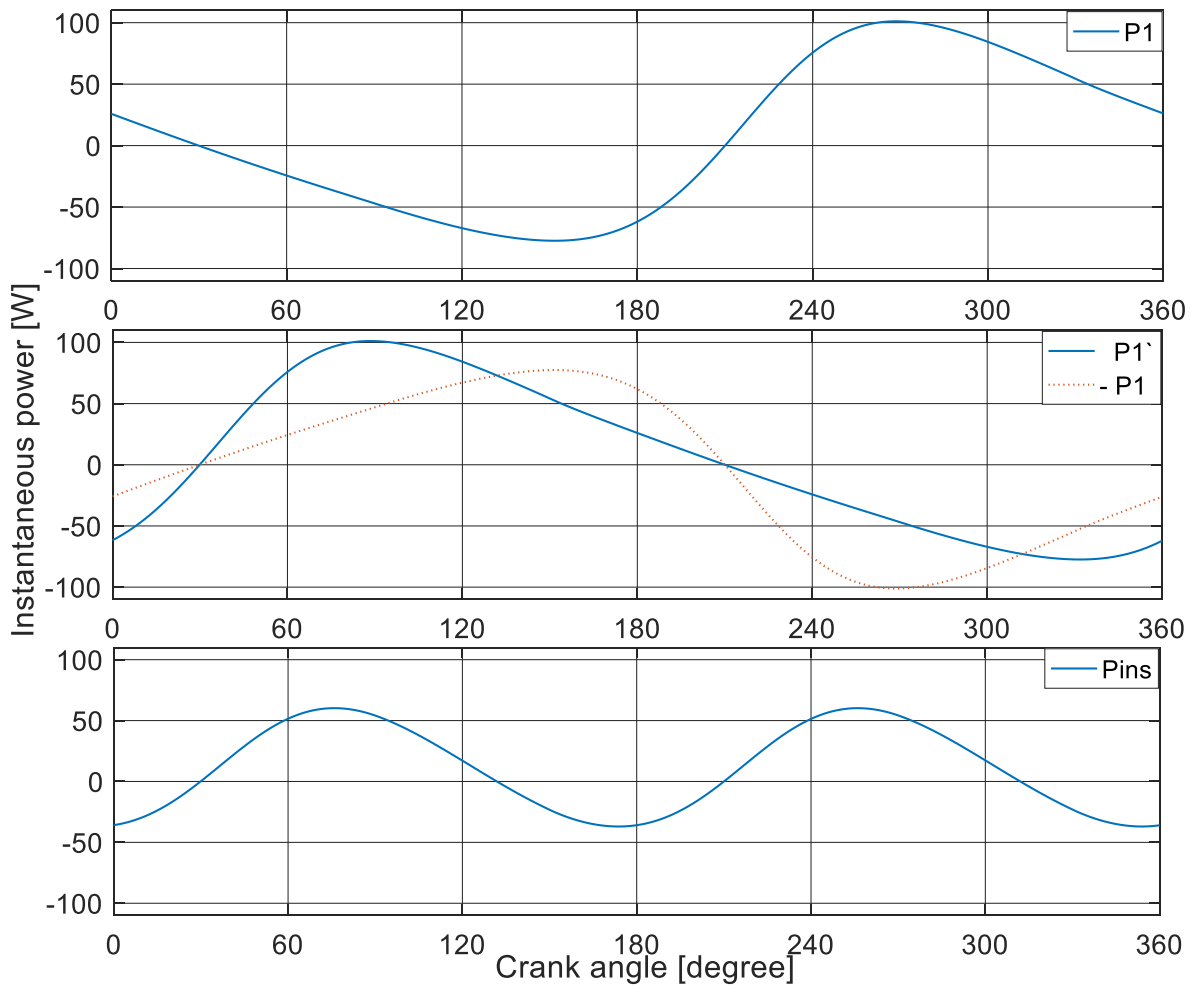
265

266

267

268

Figure 7 shows that the instantaneous powers of the opposite Stirling engines do not negate each other because otherwise, the generated power would be zero. The frequency of the combined power signal P_{ins} of the double acting Franchot engine is twice the frequency of an alpha engine because the individual instantaneous powers are not sinusoidal and the shifted power peaks do not match with the original peaks. Høeg et al. [10] also showed that the torque signal frequency is twice the engine rotation frequency. Therefore, the Franchot engine has two negative power regions in one rotation, which are smaller in magnitude than the negative power of a duplicated alpha engine. In a duplicated alpha engine, the negative powers are added together whilst in the Franchot engine, negative and positive powers are added which reduces the power variations hence torsional vibrations.

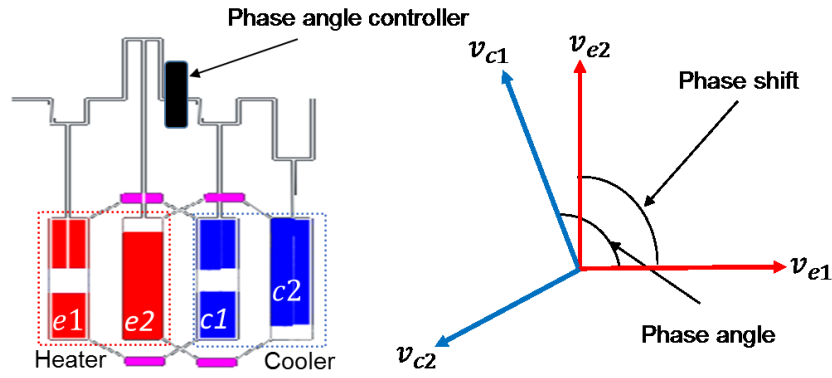


269

270 *Figure 7: Instantaneous power response at the steady state of the reference engine showing the power of one side, the*
 271 *difference between the shifted and negated power and the total instantaneous power of the reference Franchot engine.*

272 **3.2 Dual phase (2-ph) Franchot engine**

273 The dual Franchot engine is comprised of two Franchot engines connected to a slider crank drive in
 274 inline topology. The dual Franchot engine can be mechanically coupled to the crankshaft in inline
 275 configurations where there is an arbitrary phase shift between any of the two hot or cold cylinders.
 276 Figure 8 shows a dual Franchot engine for which the phase angle can be controlled with a single device
 277 and which uses a common heater and a common cooler. The phasor diagram in Figure 8 shows that
 278 the dual Franchot engine is prone to vibrations due to the uneven distribution of cranks and masses
 279 unless the phase shift is set to 180°. However, at a phase shift of 180° or multiples thereof, the
 280 thermodynamic performance of the dual engine is similar to the 1-ph engine (see Figure 9).

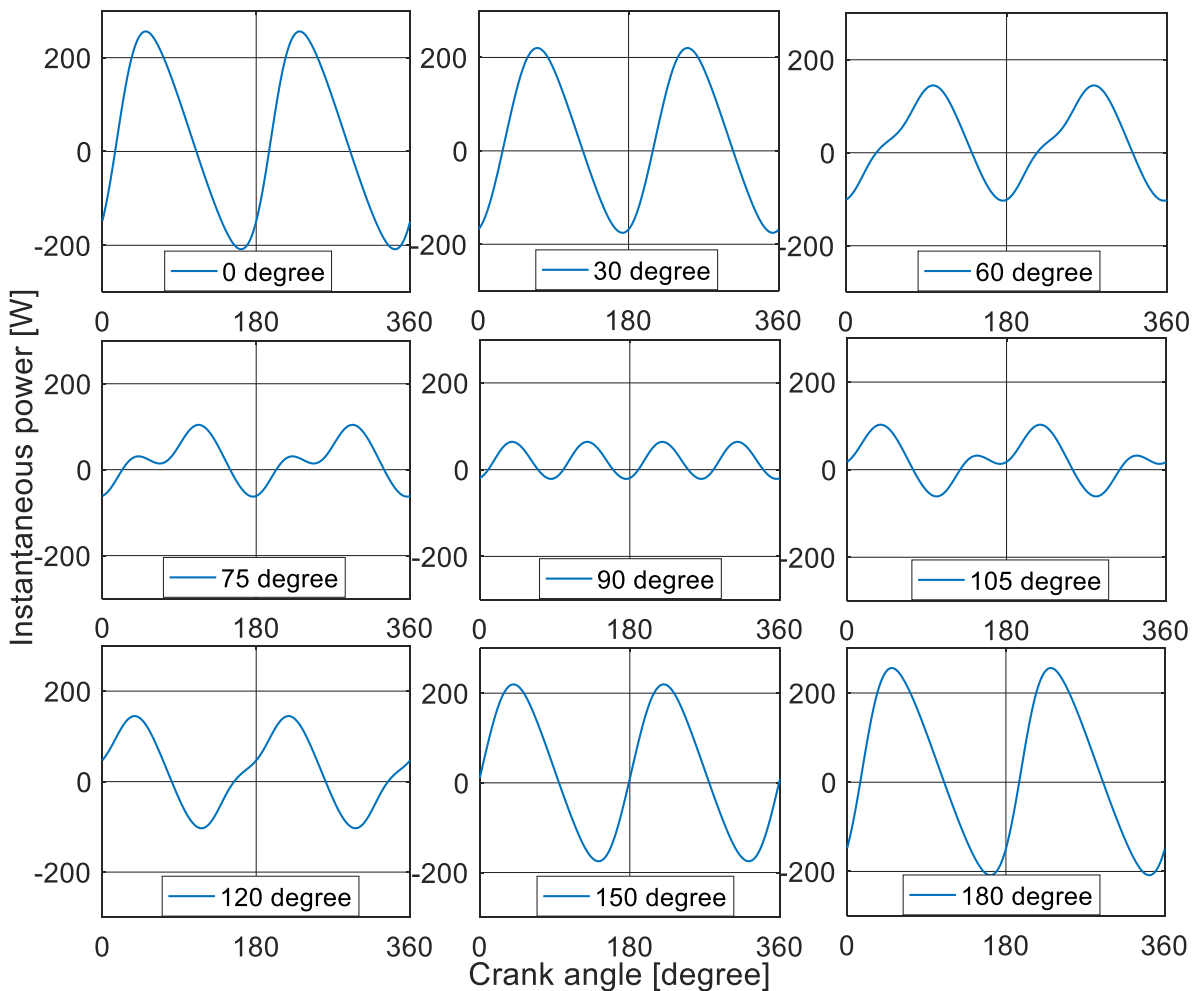


281

282

Figure 8: Dual kinematic Franchot engine and its phasor diagram.

283 Figure 9 shows that the lowest power variation occurs at the 90° phase shift. The same angle was
 284 confirmed experimentally for causing the minimum torque variations by Høeg et al. [10]. Thus, the
 285 dependency on a flywheel is reduced and the self-starting properties are better than for the 1-ph
 286 Franchot engine, although small negative power durations still exist at the studied speed.



287

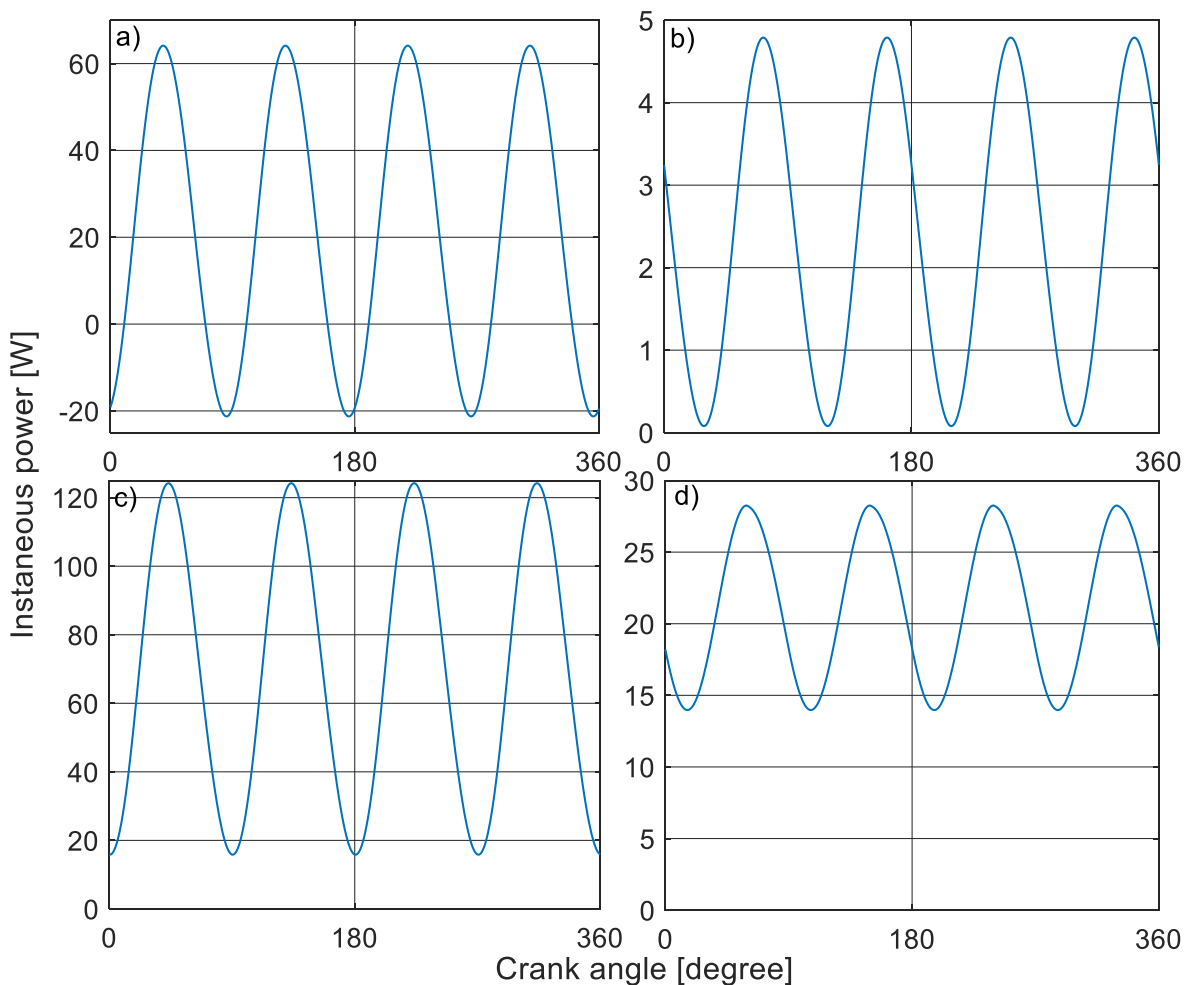
288

Figure 9: Effect of the phase shift on the power variation of a 2-ph Franchot engine at 90° phase angle.

289 The largest reduction in power variation occurs when the instantaneous powers of two Franchot
 290 engines are added with a 180° shift in power signal. In this case, each negative power duration is
 291 matched with a positive power duration in the opposite engine. The 180° shift in power signal is

292 achieved for a 90° phase shift because the power wave frequency is twice the engine rotation
 293 frequency (see Figure 7). At a 90° phase shift, the power frequency of the 2-ph engine is four times
 294 the rotation frequency. Similarly, the phase shifts of 0° and 180° produce 0° and 360° phase shifts in
 295 the power wave, respectively and thus no shift in the power signal. Therefore, two or more engines
 296 with 0° or 180° phase shift are just a 1-ph Franchot engine with multiple cylinders.

297 Figure 10 shows the capability of the 2-ph Franchot engine with a phase shift of 90° to self-start. This
 298 finding is in line with former studies [9][10][11]. The low speed represents the response of the system
 299 just after starting. At low speed, the compression process is almost isothermal due to the long cycle
 300 time, which reduces the negative power needed for compression. Thus, the engine will continue
 301 running beyond 30 RPM with a flywheel as the negative power duration vanishes at low speeds.
 302 Increasing the temperature to 600K leads to an increase in power variations as well as in the average
 303 power. Hence, the positive shift in the average power removed the negative power durations.
 304 However, most important is the phase angle which acts as a filter of the power signal by reducing the
 305 pressure variations and hence the power variations. The instantaneous power for the increased phase
 306 angle of 120° leads to a uniform positive power, which has no negative durations. Hence, the 2-ph
 307 Franchot engine can be self-starting as the negative power durations vanish for increased temperature
 308 difference, decreased speed or increased phase angle. However, the engine is still generating power
 309 pulses, which makes the engine dependent on a flywheel to run smoothly, and the cranks are still
 310 unevenly distributed.

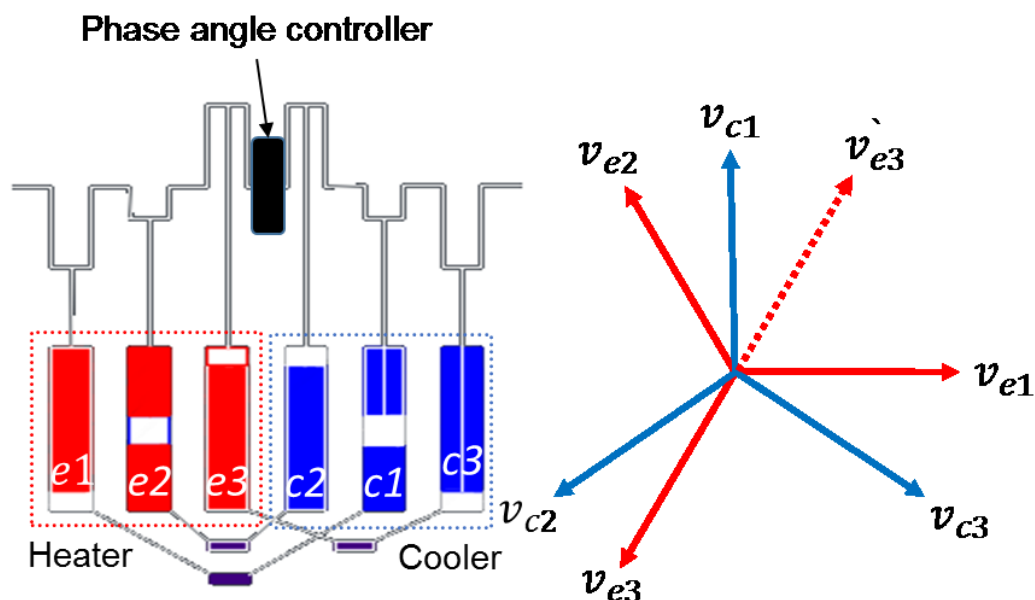


311

312 *Figure 10: Instantaneous power of dual Franchot engine at phase shift of 90° and a) phase angle of 90° b) phase angle of*
 313 *90° and $n = 30$ rpm c) phase angle of 90° and $T_h = 600$ K d) reference engine at phase angle of 120° .*

314 **3.3 Three phase (3-ph) Franchot engine**

315 The 3-ph Franchot engine shown in Figure 11 is arranged in an inline topology in the slider crank
 316 mechanism so that there are a common heater, a common cooler and one device to control the phase
 317 angle. As each Franchot engine has two regenerators, this arrangement has a twin of longer
 318 regenerator connections between cylinder e1 and c1 in comparison to the other connections. The
 319 phasor diagram (Figure 11) shows a uniform distribution of the masses and forces on the crankshaft
 320 which removes the vibrations caused by the unbalanced forces and masses. The phasor diagram
 321 shows the reciprocal vibrations vanish even if the phase angle is controlled as the vector summation
 322 of the forces is zero for arbitrary phase angles. In addition, it is also possible to remove the rocking
 323 couples if the phase angle equals the phase shift. At this phase angle, the engine has piston twins (e1-
 324 c3, e2-c1 and e3-c2) that move with each other. Therefore, to reduce the primary vibrations, both the
 325 phase shift and phase angle have to be fixed to 120°. By swapping the location of cold cylinders c1 and
 326 c2 the engine would have equal regenerator lengths but the rocking couples will not be inherently
 327 removed.

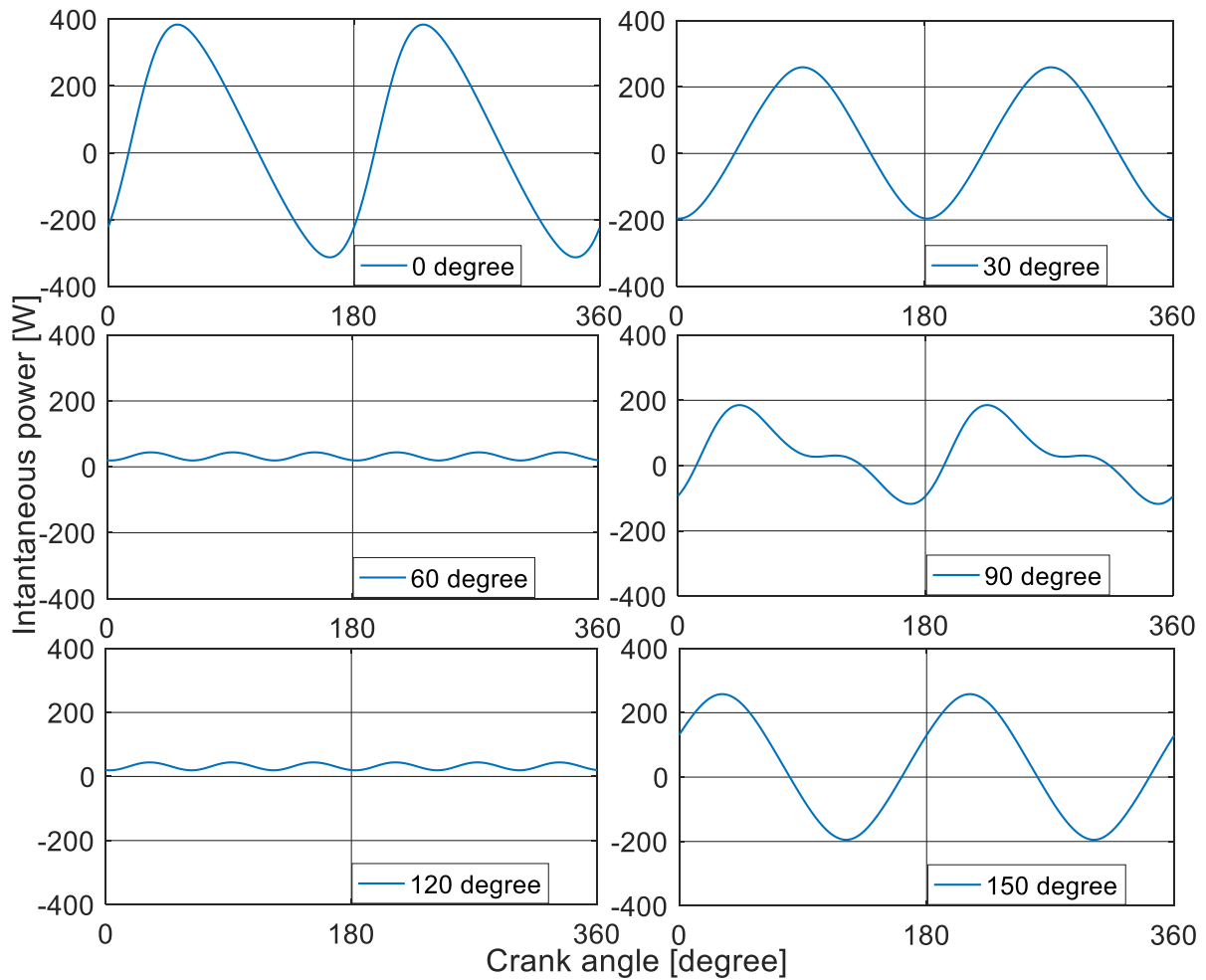


328

329

Figure 11: 3-ph kinematic Franchot engine and its phasor diagram.

330 Figure 12 shows that there are two phase shifts (60° and 120°) at which the system has the minimum
 331 power variation. At these angles, the power frequency is three times the power pulse frequency or six
 332 times the rotational frequency of a 1-ph Franchot engine. The minimum instantaneous power is
 333 shifted to a positive value and the power variation on the crankshaft is reduced.



334

335

Figure 12: Effect of the phase shift on the instantaneous power of the 3-ph Franchot engine at 90° phase angle.

336

337

338

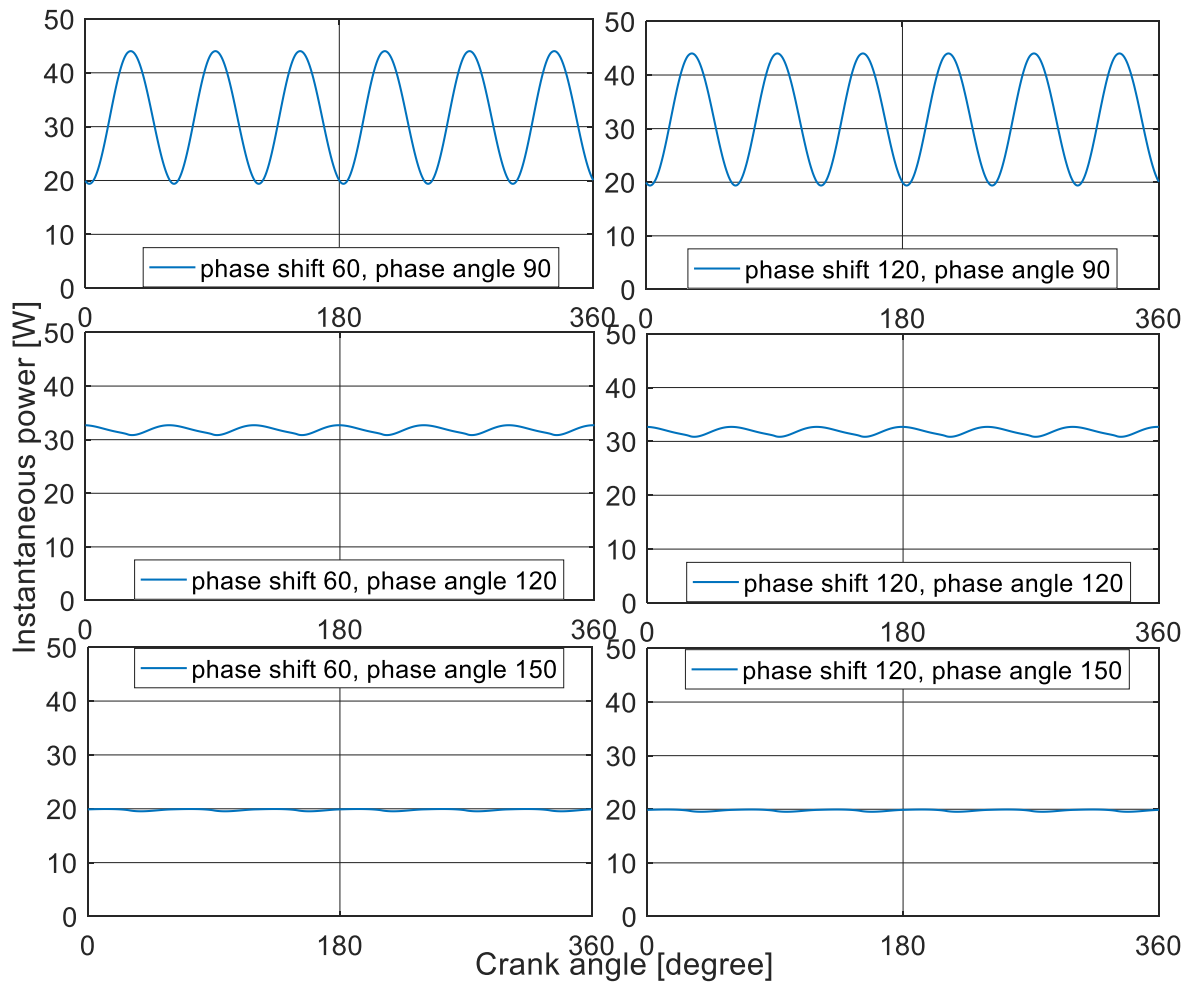
339

340

341

342

Figure 13 shows the power response of the 3-ph Franchot engine is similar at phase shifts of 60° and 120° for different phase angles. The reason for this is that the Franchot engine has two Stirling engines mounted mechanically opposite to each other and thus, the 60° corresponds to 120° for the opposite engine as it is shifted by 180° (see Figure 11). In addition, larger phase angles lead to smaller power variations hence smoother power signals. These power variations are much smaller than in the 2-ph Franchot engine (see Figure 9). Therefore, the need for a flywheel is much smaller for the 3-ph Franchot engine than for the 2-ph engine.



343

344 *Figure 13: Effect of the phase angle on the power variation of a 3-ph Franchot engine at 60° and 120° phase shifts.*

345 **3.4 Multi-phase ($n - ph$) Franchot engine**

346 The different power signals of a multi-phase engine are added to the crankshaft. As seen in Figure 7,
 347 the 1-ph engine has a power frequency, which is two times the engine rotational frequency and thus
 348 each phase has two maxima and two minima in one cycle. In order to remove the negative power
 349 durations, each negative power duration must be balanced by positive power durations. In the multi-
 350 phase engine, the phase shifts can be chosen with the aim of cancelling the maxima and minima.

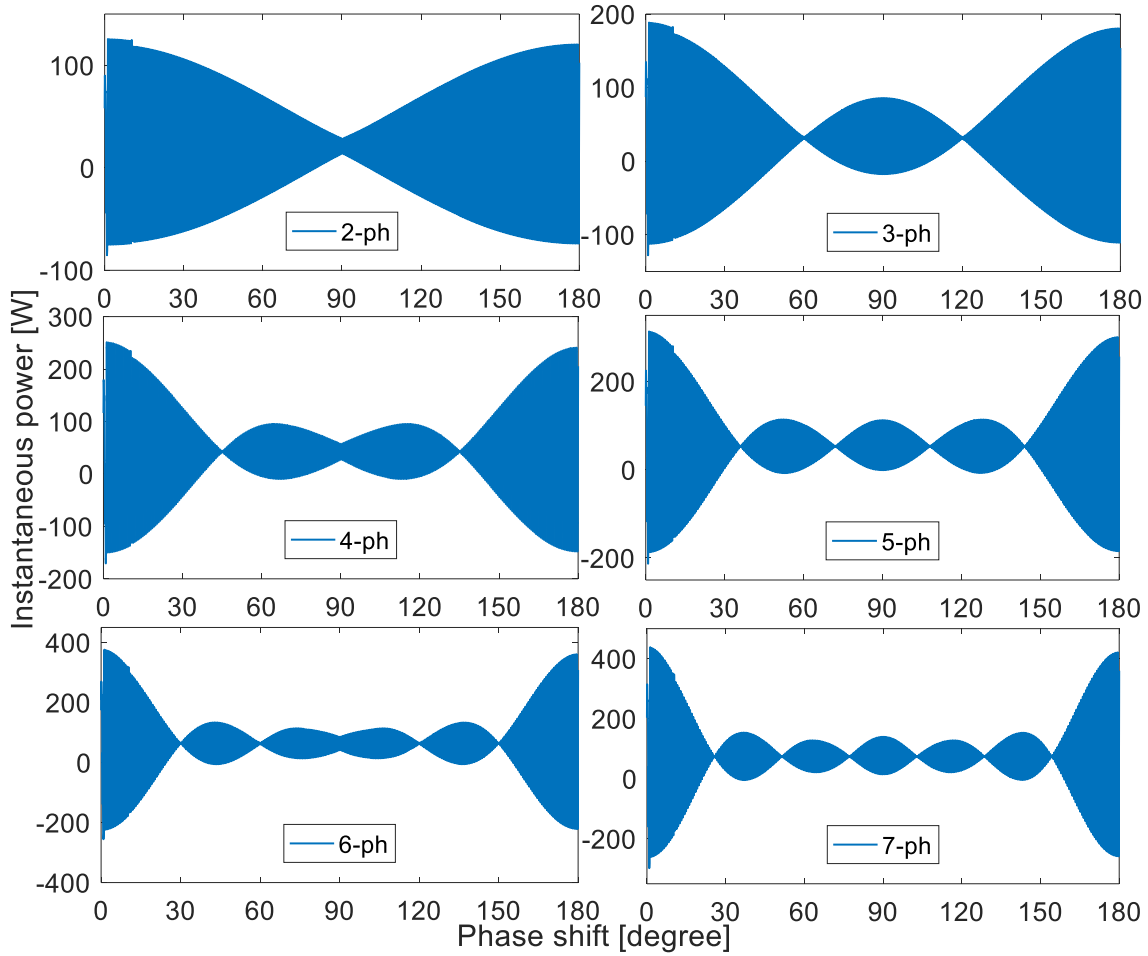


Figure 14: Power amplitude response of the multi-phase Franchot engine with the phase shift.

351

352

353 Figure 14 shows the power amplitude for the 2-ph to 7-ph Franchot engines over the phase shift. For
 354 each $n - ph$ engine, there are $n - 1$ different phase shifts which produce power variation minima.
 355 The phase shifts that lead to the lowest power variations are given by

$$\theta_s = \frac{180}{n} y \quad 32$$

356

357 where y is an integer between 1 and $n - 1$, n is the number of phases (pair of hot and cold cylinders)
 358 of the Franchot engine. For even y values, the Franchot engines will be uniformly distributed around
 359 the crankshaft making a symmetric phase shift between the adjacent engines. The minimum phase
 360 shift of the uniformly distributed $n - ph$ Franchot engine is twice the phase shift of an equivalent
 361 Siemens configuration and is given by

$$\theta_s = \frac{360}{n} \quad 33$$

362

363 For odd y values, the Franchot engines will be stacked on one half of the crankshaft making the
 364 smallest phase shift equal to

$$\theta_s = \frac{180}{n} \quad 34$$

365

366 Those two phase shifts have the same effect on the power signal because each Stirling engine in a
 367 Franchot engine completes a power cycle in one rotation and the two power cycle are shifted by 180° .
 368 In another word, the power cycle frequency of a Franchot engine is twice that of the Stirling engine
 369 which makes each Franchot engine complete a power signal cycle in half a rotation. As the power is
 370 non-dimensional and due to the Franchot opposite engines, the instantaneous power at a phase shift
 371 of θ is equivalent to the instantaneous power at $180^\circ - \theta$ and hence, it is mirrored about 90° . At the
 372 phase shift of 90° , the angular shift in the power signal is $180n$. Hence, for an even number of phases
 373 this results in a signal duplication for which the signal amplitude is amplified instead of being filtered.

374 Since the phase shift is valid for $y \leq n - 1$, the minimum number of phases that results in power
 375 minima and have symmetric distribution is three since y needs to be an even number. Symmetric
 376 distribution of phases uniformly distributes the forces and masses on the crankshaft, which reduces
 377 the vibrations encountered by them. In order to reduce the vibrations related to the rocking couples,
 378 there should be pairs of expansion and compression pistons that move simultaneously in the same
 379 direction. Thus, the phase angle must be fixed based on the phase shift. However, for $n > 4$, different
 380 phase angles can be obtained due to the regenerator connections. For example, for $n = 5$ the
 381 expansion volume $v_{e,k}$ might be connect to the compression volume $v_{c,k+1}$ or $v_{c,k+2}$ which would
 382 result in different phase angles.

383 Table 3 summarises the potential phase angles up to the $8 - ph$ Franchot engine where the phases
 384 are uniformly distributed around the crankshaft. These phase angles can be mathematically described
 385 by Equation 32, which is also used to calculate the phase shift, but only for even y . These phase angles
 386 are similar to the phase angles of the multi-cylinder single-acting Stirling engine [7].

387 *Table 3: Phase angle of the multi cylinder Franchot engine*

	3-ph	4-ph	5-ph	6-ph	7-ph	8-ph
y=2	120°	90°	72°	60°	51.4°	45°
y=4			144°	120°	102.8°	90°
y=6					154.2°	135°

388 4 Conclusion

389 The phasor diagram and a reduced multi-cylinder model are used to obtain the power signal to
 390 evaluate the vibrations and self-starting capabilities of multi-cylinder Franchot engines. The polytropic
 391 model shows good agreement with the performance curves from a published experimental study. It
 392 is shown that the multi-cylinder Franchot engines are self-starting if at least two Franchot engines are
 393 combined. In addition, the cranks can be evenly distributed for three or more Franchot engines.
 394 Finally, the power oscillation can be reduced for the $n - ph$ engine, which agrees with the reported
 395 cases. Hence, the slider crank mechanism is recommended for the $n - ph$ Franchot engine where $n \geq$
 396 3 as it is able to reduce the power pulses, rocking couples and primary vibrations caused by each
 397 Franchot engine on the rotating crankshaft. On the other hand, the slider crank mechanism does not
 398 remove the rocking couples in the Siemens configuration. In addition, the 3-ph Franchot engine gives
 399 a preferable phase angle of 120° in contrast to 60° of an equivalent Siemens configuration. Thus, the
 400 multi-cylinder Franchot engine can be self-starting, has significantly reduced vibrations and can use
 401 the simple slider crank mechanism.

402 Acknowledgement

403 The authors would like to thank the British Council - HESPAL for the Ph.D scholarship for Jafar M.
404 Daoud.

405 **References**

- 406 [1] G. Walker, "Coal-fired Stirling engines for railway locomotive and stationary power
407 applications," *Proc Instn Mech Engrs*, vol. 197A, no. October, pp. 233–246, 1983.
- 408 [2] B. Hoegel, D. Pons, M. Gschwendtner, and A. Tucker, "Theoretical investigation of the
409 performance of an Alpha Stirling engine for low temperature applications," *ISEC Int. Stirling
410 Engine Comm.*, no. January, 2012.
- 411 [3] M. H. Ahmadi, M.-A. Ahmadi, and F. Pourfayaz, "Thermal models for analysis of performance
412 of Stirling engine: A review," *Renew. Sustain. Energy Rev.*, vol. 68, no. October 2016, pp. 168–
413 184, 2017.
- 414 [4] D. G. Thombare and S. K. Verma, "Technological development in the Stirling cycle engines,"
415 *Renew. Sustain. Energy Rev.*, vol. 12, no. 1, pp. 1–38, Jan. 2008.
- 416 [5] G. Fenies, F. Formosa, J. Ramousse, and A. Badel, "Double acting Stirling engine: Modeling,
417 experiments and optimization," *Appl. Energy*, vol. 159, pp. 350–361, 2015.
- 418 [6] G. Walker, *Cryocoolers*, Part 1: Fu. Boston, MA: Springer US, 1983.
- 419 [7] S. Chatterton and P. Pennacchi, "Design of a Novel Multicylinder Stirling Engine," *J. Mech. Des.*,
420 vol. 137, no. 4, p. 042303, 2015.
- 421 [8] D. M. Berchowitz and Y.-R. KWon, "Multiple-cylinder, free-piston, alpha configured Stirling
422 engines and heat pumps with stepped pistons," U.S. Patent 7,171,811 B1, 2007.
- 423 [9] J. Arthur A. Varela, "Hybrid electric propulsion system," U.S. Patent 5,172,784 A, 1992.
- 424 [10] A. Høeg, T.-M. Tveit, T. Aase, and T.-A. Asphjell, "Mechanical Design of the 4-500 KWth stirling
425 cycle heat pump SPP 4-106," in *The 17th International Stirling Engine Conference*, 2016, pp.
426 21–33.
- 427 [11] P. Fette, "A Stirling Engine Able to Work with Compound Fluids Using Heat Energy of Low to
428 Medium Temperatures," in *Sixth International Stirling Engine Conference*, 1993, pp. 13–18.
- 429 [12] T. Finkelstein, "Optimization of phase angle and volume ratio for Stirling engines," Jan. 1960.
- 430 [13] T. Finkelstein and A. J. Organ, *Air Engines*. 2001.
- 431 [14] M. A. White, J. E. Augenblick, and A. A. Peterson, "Double acting thermodynamically resonant
432 free-piston multicylinder Stirling system and method," U.S. Patent 7,134,279 B2, 2006.
- 433 [15] B. Hoegel, "Thermodynamics-based design of stirling engines for low-temperature heat
434 sources.," University of Canterbury, 2014.
- 435 [16] H. Damirchi, G. Najafi, S. Alizadehnia, R. Mamat, C. S. Nor Azwadi, W. H. Azmi, and M. M. Noor,
436 "Micro Combined Heat and Power to provide heat and electrical power using biomass and
437 Gamma-type Stirling engine," *Appl. Therm. Eng.*, vol. 103, pp. 1460–1469, 2016.
- 438 [17] C. Çınar, F. Aksoy, H. Solmaz, E. Yılmaz, and A. Uyumaz, "Manufacturing and testing of an A-
439 type Stirling engine," *Appl. Therm. Eng.*, vol. 130, pp. 1373–1379, 2018.
- 440 [18] H. Karabulut, "Dynamic model of a two-cylinder four-stroke internal combustion engine and
441 vibration treatment," *Int. J. Engine Res.*, vol. 13, no. 6, pp. 616–627, Dec. 2012.

- 442 [19] D. Ipci and H. Karabulut, "Thermodynamic and dynamic modeling of a single cylinder four
443 stroke diesel engine," *Appl. Math. Model.*, vol. 40, no. 5–6, pp. 3925–3937, 2016.
- 444 [20] T. K. Garrett, K. Newton, and W. Steeds, "Engine balance," in *Motor Vehicle*, Elsevier, 2000, pp.
445 25–46.
- 446 [21] J. M. Daoud and D. Friedrich, "Performance investigation of a novel Franchot engine design,"
447 *Int. J. Energy Res.*, Aug. 2017.
- 448 [22] J. M. Daoud and D. Friedrich, "Parametric Study of an Air Charged Franchot Engine with Novel
449 Hot and Cold Isothermalizers," *Inventions*, vol. 2, no. 4, p. 35, Dec. 2017.
- 450 [23] J. M. Daoud and D. Friedrich, "A novel Franchot engine design based on the balanced
451 compounding method," *Energy Convers. Manag.*, vol. 169, pp. 315–325, Aug. 2018.
- 452 [24] J. Mou and G. Hong, "Startup mechanism and power distribution of free piston Stirling engine,"
453 *Energy*, vol. 123, pp. 655–663, Mar. 2017.
- 454 [25] M. Pfabe and C. Woernle, "Reducing torsional vibrations by means of a kinematically driven
455 flywheel - Theory and experiment," *Mech. Mach. Theory*, vol. 102, pp. 217–228, 2016.
- 456 [26] M. Costea and M. Feidt, "The effect of the overall heat transfer coefficient variation on the
457 optimal distribution of the heat transfer surface conductance or area in a Stirling engine,"
458 *Energy Convers. Manag.*, vol. 39, no. 16–18, pp. 1753–1761, Nov. 1998.
- 459 [27] F. Toda, S. Iwamoto, M. Matsuo, and Y. Umezane, "Heat Transfer on a Small Stirling Engine," *J.*
460 *Mar. Eng. Soc. JAPAN*, vol. 25, no. 6, pp. 358–365, 1990.
- 461 [28] H. Karabulut, H. S. Yucesu, and A. Koca, "Manufacturing and testing of a V-type Stirling engine,"
462 *Turkish J. Eng. Environ. Sci.*, vol. 24, no. 2, pp. 71–80, 2000.
- 463 [29] C. H. Cheng and Y. J. Yu, "Numerical model for predicting thermodynamic cycle and thermal
464 efficiency of a beta-type Stirling engine with rhombic-drive mechanism," *Renew. Energy*, vol.
465 35, no. 11, pp. 2590–2601, 2010.
- 466 [30] B. Kongtragool and S. Wongwises, "Thermodynamic analysis of a Stirling engine including dead
467 volumes of hot space, cold space and regenerator," *Renew. Energy*, vol. 31, no. 3, pp. 345–359,
468 Mar. 2006.
- 469 [31] M. Tanaka, I. Yamashita, and F. Chisaka, "Flow and Heat Transfer Characteristics of the Stirling
470 Engine Regenerator in an Oscillating Flow," *JSME Int. J.*, vol. 33, no. 2, pp. 283–289, 1990.
- 471 [32] M. Babaelahi and H. Sayyaadi, "Simple-II: A new numerical thermal model for predicting
472 thermal performance of Stirling engines," *Energy*, vol. 69, pp. 873–890, May 2014.
- 473